PAPER

Chiral near-fields around chiral dolmen nanostructure

IOP Publishing Journal of Physics D: Applied Physics

J. Phys. D: Appl. Phys. **50** (2017) 474004 (6pp) https://doi.org/10.1088/1361-6463/aa8f81

Chiral near-fields around chiral dolmen nanostructure

Tong Fu, Tiankun Wang, Yuyan Chen, Yongkai Wang, Yu Qu and Zhongyue Zhang

School of Physics and Information Technology, Shaanxi Normal University, Xi'an 710062, People's Republic of China

E-mail: zyzhang@snnu.edu.cn

Received 8 June 2017, revised 24 September 2017
Accepted for publication 27 September 2017
Published 3 November 2017

Abstract

Discriminating the handedness of the chiral molecule is of great importance in the field of pharmacology and biomedicine. Enhancing the chiral near-field is one way to increase the chiral signal of chiral molecules. In this paper, the chiral dolmen nanostructure (CDN) is proposed to enhance the chiral near-field. Numerical results show that the CDN can increase the optical chirality of the near-field by almost two orders of magnitude compared to that of a circularly polarized incident wave. In addition, the optical chirality of the near-field of the bonding mode is enhanced more than that of the antibonding mode. These results provide an effective method for tailoring the chiral near-field for biophotonics sensors.

Keywords: chiral near-field, chiral sensing, circular dichroism

(Some figures may appear in colour only in the online journal)

Introduction

Chiral structures have opposite handedness with respect to their mirror images [1, 2]. As a result, radiation of different handedness e.g. circularly polarized (CP) light or a structured light with orbital angular momentum [3] have a different transmission and reflection in chiral materials. Due to this property, the measurement of circular dichroism (CD) became an incisive technique for the detection of chiral molecules [1, 4–6]. For example, optical detection of the chiral molecules of β-structured amyloid plaque has found useful application in the diagnosis of Alzheimer's and Parkinson's diseases [7]. Experimentally, the signal-to-noise ratio is low, because the molecule dipole moment is small in comparison with the chiral pitch of a CP wave. Despite the CD spectrum of the chiral molecule being located in the ultraviolet band, when there is interaction with plasmonic nanostructures, the chiral optical properties of the molecule can be brought into the visible region and enhanced through two means. First, induced current in achiral plasmonic structure by chiral media can lead to a chiroptical response in the plasmon range, namely the induced CD [8]. Besides, considering the chiral media as an effective index, when the chiral media are in the vicinity of the chiral plasmonic structure, redshift of CD spectra of the chiral plasmonic structure can occur in the plasmon range [7].

When the chiral molecule is located in the vicinity of the chiral plasmonic nanostructure, the relative strength of the chiral signal will be enhanced [7]. Superchiral fields can be generated in some region of space, such as the node of a standing wave formed by a CP wave and chiral plasmonic nanostructures [9–13]. When the chiral molecule is located in this region its relative chiral signal will be enhanced. The chiral near-field is the local field at each point around the nanostructure, in contrast to the far-field radiation measured via CD. The optical chirality C is a time-even pseudoscalar defined as [14]

$$C \equiv \frac{\varepsilon_0}{2}\mathbf{E}\cdot\nabla\times\mathbf{E}+\frac{1}{2\mu_0}\mathbf{B}\cdot\nabla\times\mathbf{B}, \tag{1}$$

where $\mathbf{E}$ and $\mathbf{B}$ are the electric and magnetic fields, respectively. ε_0 and μ_0 represent the vacuum permittivity and permeability, respectively. A simpler type of C can be deduced as [15]

$$C=\frac{\varepsilon_0\omega}{2}\mathrm{Im}\left(\mathbf{E}_\mathrm{C}^*\cdot\mathbf{B}_\mathrm{C}\right). \tag{2}$$

Note that $\mathbf{E}_\mathrm{C}$ and $\mathbf{B}_\mathrm{C}$ in equation (2) denote the complex electric and magnetic field, respectively, while only the real parts

are considered in equation (1). And ω is the angular frequency of $\mathbf{E}_C$ and $\mathbf{B}_C$. Note that $\mathbf{E}_C$ and $\mathbf{B}_C$ need to have a collinear part and phase difference to obtain non-zero optical chirality, and particularly when $\mathbf{E}_C$ and $\mathbf{B}_C$ are collinear and have a $\pi/2$ phase difference, the chirality reaches its maximum. For the plane wave, the maximum optical chirality is obtained from CP waves as

$$C_{\mathrm{CP}}^{\pm} = \pm \frac{\varepsilon_0 \omega}{2c} |\mathbf{E}|^2, \tag{3}$$

where $+$ and $-$ denote left-handed circularly polarized (LCP) and right-handed circularly polarized (RCP) waves, respectively, and c is the speed of light in the vacuum. The enhancement of the chiral near-field had been achieved with numerous metallic structures under different polarizations of incident wave [15–19]. Recent study on local CD and thermally-controlled chirality may open new opportunities for dynamic detection of the chiral molecules [20, 21].

Usually, the chirality of a chiral structure is determined by its CD spectrum [22], but for the enhancement of chiral signal the chirality is determined by the local field. According to equation (2), the chiral near-field is proportional to the imaginary part of $\mathbf{E}_C^* \cdot \mathbf{B}_C$, which results in two different aspects that should be considered when optimizing the chiral near-field: on the one hand, the chiral near-field will increase and the included angle between the electric and magnetic fields decreases. On the other hand, enhancing complex local electric and magnetic fields will increase the optical chirality as well. Under the former condition, the maximum chiral near-field is contributed by parallel or anti-parallel electric and magnetic fields. Thus, an ideal choice is a helical plasmonic nanoantenna, which has parallel electric and magnetic fields [15].

In this paper, we propose a chiral dolmen nanostructure (CDN) to obtain strong C enhancement. Compared with conventional devices, CDN possesses strong chiral near-field, which is distributed mainly on the surface of the nanostructures and is thus more applicable. Simulation results reveal that the CDN reaches two orders of magnitude enhancement of the chiral near-field with respect to CP waves. It is noteworthy that the chiral plasmonic bonding mode of the CDN enhances the chiral near-field compared to the plasmonic anti-bonding mode. Hence, the chiral near-field can be tailored by the geometric parameters of the CDN.

Structure and simulation method

CDN is a periodic nanostructure with a fixed period of 200 nm both at the x and y directions, as shown in figure 1. Two parallel nanorods have the same length of L_1, and the perpendicular rod has a length of L_2. The widths of all the nanorods are w. The separation between the two parallel nanorods and the perpendicular rod is s. The heights of the rods are h_1, h_2 and h_3, respectively, and $h_1 < h_2 < h_3$ for L-CDN, as shown in figure 4(b). The chiral structures are excited with normal incidence of LCP and RCP waves. CD is defined as $\mathrm{CD} = A_- - A_+$, where A_- and A_+ denote the absorption under LCP and RCP wave illumination, respectively.

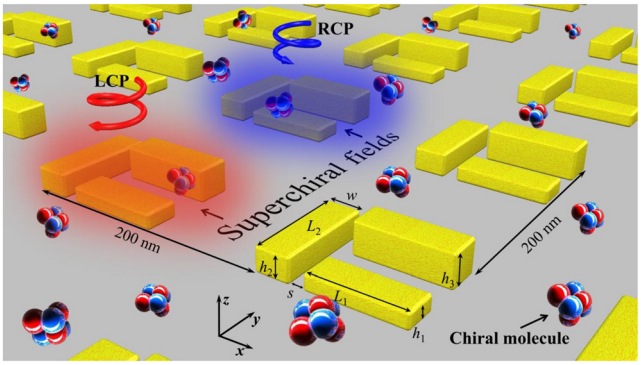

Figure 1. Schematic of enhancing chiral signal with CDN and the parameters of CDN.

The finite element method software COMSOL Multiphysics is used to perform the simulation. The refractive index of gold is taken from experimental data in [23]. To observe the enhancement with respect to CP waves, the chiral near-field of the chiral structures is normalized by CP waves:

$$\hat{C} \equiv \frac{C}{|C_{\mathrm{CP}}|} = -\frac{c\mathrm{Im}(\mathbf{E}_C^* \cdot \mathrm{B}_C)}{|\mathbf{E}_{\mathrm{CPL}}|^2}. \tag{4}$$

Results and discussion

The far-field response of absorption and CD spectra of the CDN were calculated with parameters of $L_1 = 110$ nm, $L_2 = 120$ nm, $w = 40$ nm, $h_1 = 20$ nm, $h_2 = 30$ nm, and $h_3 = 40$ nm, which are shown in figure 2(a). The absorption spectra show pronounced plasmonic resonance at approximately 690 and 810 nm for both LCP and RCP wave excitations, respectively, which is the destructive interference between bright and dark modes. The resonance wavelengths are both blueshifted compared with recent study, due to the larger periodic in the CDN, and the attractive interaction between two CDNs can be ignored [24]. The surface charge distribution that corresponds to the resonance wavelength is presented in figure 2(b). It can be clearly observed that the antibonding mode and bonding mode are excited under both polarization excitations. All the bonding and antibonding modes of the CDN are located at resonance wavelengths.

The normalized chiral near-fields, namely the optical chirality of the CDN at both plasmonic modes is calculated, as shown in figures 3(b) and (c). For the bonding mode, the strong chiral near-fields are mainly distributed at the gap region. The enhanced chiral near-field of the CDN at the bonding mode is approximately 90 times with respect to CP waves, which is comparable with those of recent study [16, 17]. Moreover, the sign of optical chirality at the two gaps is reversed under different polarization of illumination, which is of great application importance as the chiral signal will be strongly enhanced under this condition. For the antibonding mode, however, the strong chiral near-fields are mainly

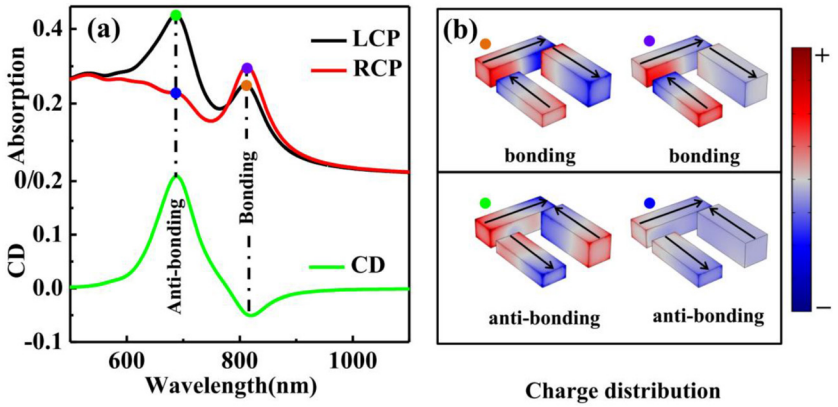

Figure 2. Optical properties of CDN. (a) Circularly polarized absorption spectra. (b) Charge distribution of CDN at wavelengths of 690 and 810 nm.

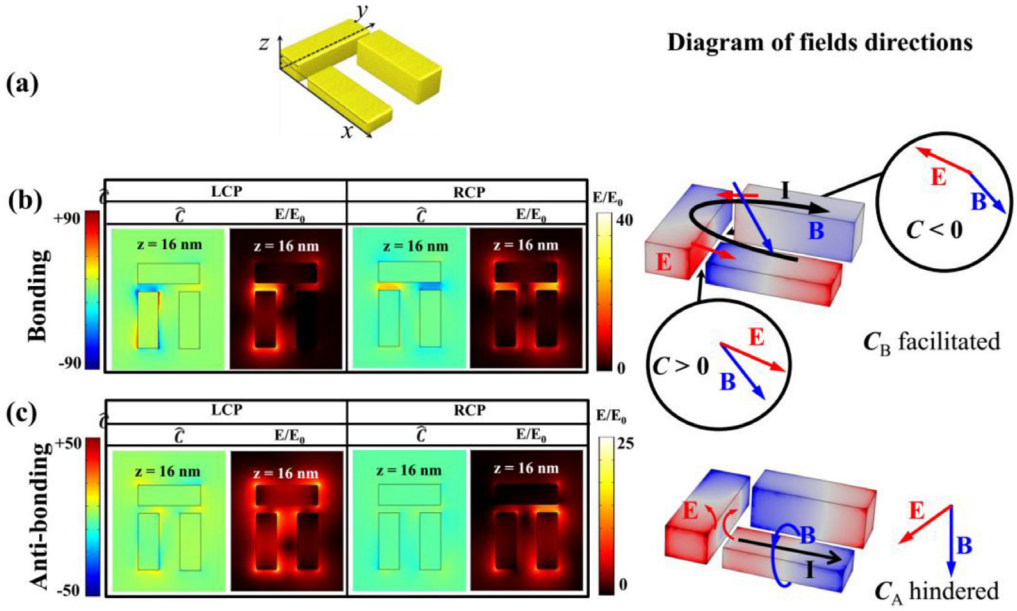

Figure 3. Chiral near-field and electric field enhancement of left-handed CDN. (a) Sketch of local field distribution plane. (b) Local chiral near-field and electric field enhancement at the bonding mode. (c) Local chiral near-field and electric field enhancement at the anti-bonding mode. Right panel shows the diagram of optical chirality at both bonding mode and antibonding mode.

distributed along the nanorods, which enhanced roughly 50 times with respect to CP waves, which is weaker than the enhancement in the bonding mode.

The reason for different enhancement at the bonding mode and antibonding mode reside in two facts. First, the electric field of the bonding mode is stronger than the anti-bonding mode. From figures 3(b) and (c), the electric field of the bonding mode is enhanced about 40 times compared to the antibonding one. However, the electric field of the anti-bonding mode is only enhanced about 25 times. Second, the angle between the electric and magnetic fields at the two gap regions of the bonding mode is smaller than the antibonding mode, as illustrated in the right panel of figures 3(b) and (c). The attractive Coulomb force is formed in the bonding mode, because the charges of opposite signs accumulate at the ends of the two rods, thus orienting the electric field parallel to the gap [25]. A magnetic field is produced, because the three electric dipoles at three nanorods with phase delay caused by the height difference can form a magnetic dipole. Therefore, the included angle between the electric and magnetic fields is small. In the bonding mode, the different sign of local chirality in the two gaps is due to the direction of the magnetic field and is not strictly along the $-z$ direction, but has an angle with respect to the $-z$ direction, because of the height difference of the nanorods. Therefore, in the left gap, the angle between the electric and magnetic field is an acute angle, but in the right gap, the angle between the electric and magnetic field is an obtuse angle (figure 3) The induced current is π out of phase with respect to the exciting field, while the induced magnetic field and induced current are in phase [26]. There is a phase shift of $\pi/2$ between the incident electric field and induced local electric field [27]. Therefore, the local magnetic and electric field are out of phase, which ensures the non-vanished chiral near-field. Given that the modes experience a repulsive Coulomb force in the antibonding state [28], the electric fields repulse each other and are perpendicular to the gap (z direction). However, the magnetic field around the electric dipole is hardly parallel to the electric field. Hence,

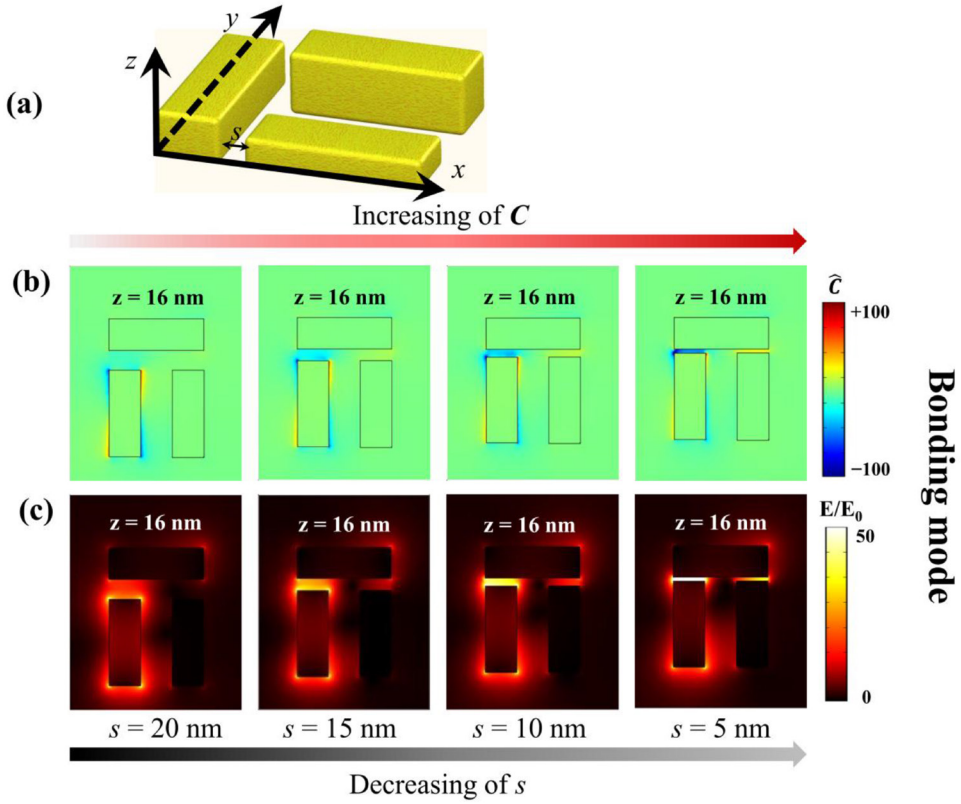

Figure 4. Local chiral near-field and local electric field enhancement under LCP excitation with different separation s at the bonding mode. (a) Sketch of dependent parameter s. (b) Chiral near-field enhancement with LCP wave excitation at the bonding mode with different s. (c) Local electric field enhancement at the bonding mode with different s.

the included angle between the electric and magnetic fields is larger than that of the bonding mode. Note that the sketches depict the optical chirality around the gap regions. Both the direction and strength of the local fields support the achievement of the strong chiral near-field in the bonding mode, but hinder it in the antibonding mode. This result is different from the intuition, as the CDN possesses a stronger CD signal at the antibonding mode (about 30%), but the maximum optical chirality resides in the bonding mode. Therefore, when detecting chiral molecules, the bonding mode should be considered rather than the antibonding mode, despite the antibonding mode's stronger CD signal.

According to equation (2), the near-field amplitude can be enhanced by manipulation of the local fields. Figure 4 shows the chiral near-field together with electric fields at the bonding mode, tailored with the change of s. Figure 4(a) gives the schematic of the illumination and the simulated parameter. Only the bonding mode was exhibited, because of its stronger field than the antibonding mode, and only one polarization of illumination was shown for another share the same condition. The chiral near-field was accordingly shown in figure 4(b). The chiral near-field increased with the decreasing of s, and was enhanced about 100 times with respect to the CP waves when $s = 5$ nm. The local electric field enhancement was simulated accordingly, as shown in figure 4(c). The same as for the chiral near-fields, the electric fields increased with decreasing the separation of s. The electric fields were enhanced by about 50 times when $s = 5$ nm, as shown in figure 4(c).

To investigate the influence of height difference on the chiral near-fields, the chiral near-field was simulated in figure 5 along with electric field enhancement. Figure 5(a) shows the schematic of the illumination and the parameter of the height difference Δh. When increasing the height difference, the chiral near-fields were decreased, as shown in figure 5(b). The electric fields decreased as well with the increasing height (figure 5(c)). The reason resides in the fact that the effective area (the cross-section with two nanorods face to face) ratios were decreased, and the accumulated electrons decreased, when increasing the height difference despite the chirality of the CDN being increased. The detection of the handedness of the chiral molecules in the CDN is based on the CD spectrum. Hence, the height difference should be chosen properly to achieve a large chiral near-field and one should also make sure that the CD of the CDN is large enough for measurement, and that the optimized height difference is about 10 nm.

Chiral molecules exist in most medicines, and chiral molecules with one handedness are useful, while chiral molecules with the other handedness are harmful. For example, ethambutol can fight tuberculosis, while its enantiomer causes blindness. The chiral signal of the chiral molecules is intrinsically weak and the CDN with enhanced local chirality can be used to distinguish the handedness of the chiral molecules. The enhanced chiral signal of the chiral medium can be detected through the CDN by taking the chiral molecules as an effective index [7]. Specifically, when it comes to experiment, one can fabricate both handedness of the CDN, and measure the CD spectra of L- and R-handed CDN in water. Then, one can

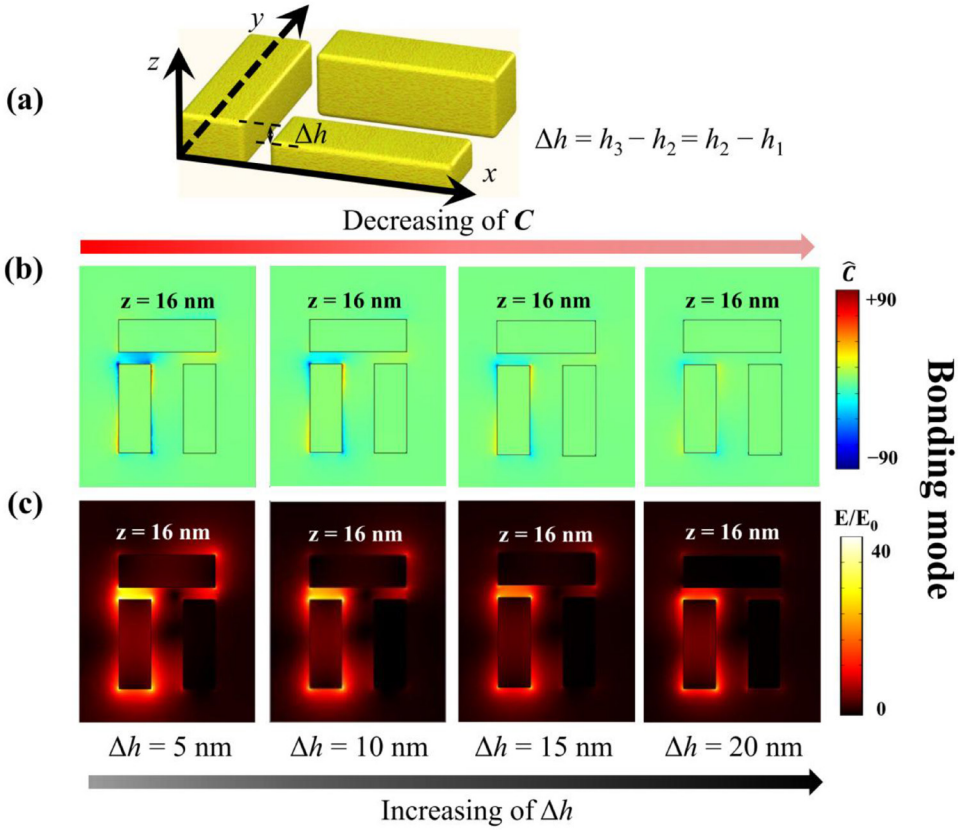

Figure 5. Local chiral near-field and local electric field enhancement under LCP with height difference of Δh at the bonding mode. (a) Sketch of dependent parameter of Δh. (b) Chiral near-field enhancement with LCP wave excitation at the bonding mode with different Δh. (b) Local electric field enhancement at the bonding mode with different Δh.

measure the L- and R-handed CDN in the chiral molecules solution. The CD spectra of the L- and R-handed CDN will redshift differently due to the chiral molecules having a different effective index when around the CDN. By calculating the redshift difference, the enhanced dissymmetry factor of the chiral molecule can be calculated.

Conclusion

The near-fields of CDNs have been calculated for different plasmonic modes. Simulation results reveal that the chiral near-field is favored at the bonding mode but hindered at the antibonding mode. Two orders of magnitude of chiral near-field enhancement have been achieved at the bonding mode. By properly adjusting the plasmonic structure and polarization state of excitation, stronger chiral near-field and large continuous regions may be achieved. These results open new experimental opportunities for the detection of chiral molecules.

Acknowledgments

This work was supported by the National Natural Science Foundation of China (NSFC) (Grant No.61575117), the Fundamental Research Funds for the Central Universities of the Ministry of Education of China (Grant No. GK201601008), the Fundamental Research Funds for the Central Universities (Grant No. 2016CSZ013), and the Foundation for Excellent PhD Dissertation of Shaanxi Normal University (Grant No. X2014YB08).

ORCID iDs

Zhongyue Zhang https://orcid.org/0000-0002-2834-429X

References

[1] Barron L D 2004 *Molecular Light Scattering and Optical Activity* (Cambridge: Cambridge University Press)
[2] Okulov A Y 2008 3D-vortex labyrinths in the near field of solid-state microchip laser *J. Mod. Opt.* **55** 241–59
[3] Okulov A Y 2008 Angular momentum of photons and phase conjugation *J. Phys. B: At. Mol. Opt. Phys.* **41** 101001
[4] Valev V K, Baumberg J J, Sibilia C and Verbiest T 2013 Chirality and chiroptical effects in plasmonic nanostructures: fundamentals, recent progress, and outlook *Adv. Mater.* **25** 2517–34
[5] Fu T, Qu Y, Wang T, Wang G, Wang Y, Li H, Li J, Wang L and Zhang Z 2017 Tunable chiroptical response of chiral plasmonic nanostructures fabricated with chiral templates through oblique angle deposition *J. Phys. Chem.* C **121** 1299–304
[6] Wang Y, Wen X, Qu Y, Fu T and Zhang Z 2016 Direct and indirect coupling mechanisms in a chiral plasmonic system *J. Phys. D: Appl. Phys.* **49** 104–9
[7] Hendry E, Carpy T, Johnston J, Popland M, Mikhaylovskiy R V, Lapthorn A J, Kelly S M, Barron L D,

Gadegaard N and Kadodwala M 2010 Ultrasensitive detection and characterization of biomolecules using superchiral fields *Nat. Nanotechnol.* **5** 783–7
[8] Govorov A O 2011 Plasmon-induced circular dichroism of a chiral molecule in the vicinity of metal nanocrystals. Application to various geometries *J. Phys. Chem.* C **115** 7914–23
[9] Tang Y and Cohen A E 2010 Optical chirality and its interaction with matter *Phys. Rev. Lett.* **104** 163901
[10] Tang Y and Cohen A E 2011 Enhanced enantioselectivity in excitation of chiral molecules by superchiral light *Science* **332** 333–6
[11] Tullius R, Karimullah A S, Rodier M, Fitzpatrick B, Gadegaard N, Barron L D, Rotello V M, Cooke G, Lapthorn A and Kadodwala M 2015 'Superchiral' spectroscopy: detection of protein higher order hierarchical structure with chiral plasmonic nanostructures *J. Am. Chem. Soc.* **137** 80–3
[12] Lipkin D M 1964 Existence of a new conservation law in electromagnetic theory *J. Math. Phys.* **5** 696–700
[13] Okulov A Y 2010 Laser singular theta-pinch *Phys. Lett.* A **374** 4523–7
[14] Bliokh K and Nori F 2011 Characterizing optical chirality *Phys. Rev.* A **83** 021803
[15] Schäferling M, Yin X, Engheta N and Giessen H 2014 Helical plasmonic nanostructures as prototypical chiral near-field sources *ACS Photonics* **1** 30–7
[16] Schäferling M, Engheta N, Giessen H and Weiss T 2016 Reducing the complexity: enantioselective chiral near-fields by diagonal slit and mirror configuration *ACS Photonics* **3** 76–84
[17] Schäferling M, Dregely D, Hentschel M and Giessen H 2012 Tailoring enhanced optical chirality: design principles for chiral plasmonic nanostructures *Phys. Rev.* X **2** 031010
[18] Davis T J and Hendry E 2013 Superchiral electromagnetic fields created by surface plasmons in nonchiral metallic nanostructures *Phys. Rev.* B **87** 085405
[19] Hendry E, Mikhaylovskiy R V, Barron L D, Kadodwala M and Davis T J 2012 Chiral electromagnetic fields generated by arrays of nanoslits *Nano Lett.* **12** 40–4
[20] Wang H, Li Z, Zhang H, Wang P and Wen S 2015 Giant local circular dichroism within an asymmetric plasmonic nanoparticle trimer *Sci. Rep.* **5** 8207
[21] Lv T T, Li Y X, Ma H F, Zhu Z, Li Z P, Guan C Y, Shi J H, Zhang H and Cui T 2016 Hybrid metamaterial switching for manipulating chirality based on VO_2 phase transition *Sci. Rep.* **6** 23186
[22] Wang Y, Deng J, Wang G, Fu T, Qu Y and Zhang Z 2016 Plasmonic chirality of L-shaped nanostructure composed of two slices with different thickness *Opt. Express* **24** 7–17
[23] Johnson P B and Christy R W 1972 Optical constants of the noble metals *Phys. Rev.* B **6** 4370
[24] Gallinet B and Martin O J F 2011 Influence of electromagnetic interactions on the line shape of plasmonic Fano resonances *ACS Nano* **5** 8999–9008
[25] Wang Y, Wen X, Qu Y, Wang L, Wan R and Zhang Z 2016 Co-occurrence of circular dichroism and asymmetric transmission in twist nanoslit-nanorod arrays *Opt. Express* **24** 16425–33
[26] Novotny L 2007 Effective wavelength scaling for optical antennas *Phys. Rev. Lett.* **26** 266802
[27] Schäferling M, Yin X and Giessen H 2012 Formation of chiral fields in a symmetric environment *Opt. Express* **24** 26326–36
[28] Osberg K D, Harris N, Ozel T, Ku J C, Schatz G C and Mirkin C A 2014 Systematic study of antibonding modes in gold nanorod dimers and trimers *Nano Lett.* **14** 49–54